VECTORIAL NON-LOCAL TOTAL VARIATION REGULARIZATION FOR CALIBRATION-FREE PARALLEL MRI RECONSTRUCTION

Stamatios Lefkimmiatis, Andres Saucedo, Stanley Osher, and Kyunghyun Sung.

University of California, Los Angeles, United States

Email:[stamatis,sjo]@math.ucla.edu, [ASaucedo,KSung]@mednet.ucla.edu

ABSTRACT

In this work we present a calibration-free parallel magnetic resonance imaging (pMRI) reconstruction approach by exploiting the fact that image structures typically tend to repeat themselves in several locations in the image domain. We use this prior information along with the correlation that exists among the different MR images, which are acquired from multiple receiver coils, to improve reconstructions from under-sampled data with arbitrary k-space trajectories. To accomplish this, we follow a variational approach and cast the pMRI reconstruction problem as the minimization of an energy functional that involves a vectorial non-local total variation (NLTV) regularizer. Further, to solve the posed optimization problem we propose an iterative algorithm which is based on a variable splitting strategy. To assess the reconstruction quality of the proposed method, we provide comparisons with alternative techniques and show that our results can be very competitive.

Index Terms— MRI, Parallel Imaging, compressive sensing, non-local regularization, NLTV.

1. INTRODUCTION

Magnetic resonance imaging (MRI) is a powerful imaging modality that is widely used in medical applications to provide anatomical and physiological information of the human body. The MRI scanners provide data that are samples of the spatial Fourier transform (a.k.a k-space) of the object that is being imaged. Since the rate that the k-space data can be collected is inherently limited by physical and physiological constraints, full sampling of the k-space can be a very time-consuming process. The relative low speed of an MRI scanning can be a limiting factor in cases where (a) it leads to an uncomfortable experience for the patient and (b) it increases the chance of image quality degradation due to the presence of motion artifacts. This has triggered the development of MRI techniques that can accelerate the scanning process by reducing the number of required measurements but without compromising the image quality.

Parallel MRI (pMRI) techniques make use of spatially distributed receiver coils to allow for fast MRI acquisition. These methods exploit the data redundancy provided by the spatial sensitivity from the different coils and allow for a significant reduction of the number of necessary k-space samples that falls below the Shannon-Nyquist rate. In general, the solution from pMRI depends on the knowledge of the spatial sensitivity functions of the multiple receiver coils, and two strategies have been adapted to cope with this requirement. The first one utilizes pre-estimated coil sensitivities or interpolation kernels derived from calibration regions, while the

second one aims to reconstruct both the underlying image and the sensitivity maps. The main drawback of the first approach is that the quality of the reconstructed image heavily depends on the accuracy of the estimated sensitivity functions. On the other hand, the joint estimation of the underlying image and the sensitivity functions corresponds to solving a non-convex problem with only local solutions, which is also very challenging.

To deal with these fundamental limitations of pMRI methods, calibration-free techniques have been introduced, such as SAKE [1] and CLEAR [2], which do not require any explicit knowledge of the sensitivity functions. While these approaches are very appealing, they come with the cost of significant computational complexity due to the low-rankness constraints that they both impose. In this work, we follow a different approach and introduce a calibration-free image domain pMRI technique which exploits the correlation of the different coil images and the non-local self-similarity property of natural images. The latter property implies that image structures tend to repeat themselves in several locations in the image domain. Specifically, we propose to formulate the MRI reconstruction problem as the optimization of a convex objective function that involves a vectorial non-local total variation (NLTV) functional.

This paper is organized as follows: in Section 2 we formulate the pMRI reconstruction problem and in Section 3 we describe our proposed non-local regularization approach. In Section 4 we introduce our pMRI reconstruction algorithm. Finally, in Section 5 we perform comparisons with alternative techniques on simulated data to assess the performance of our method.

2. PROBLEM FORMULATION

We consider MRI acquisition with M receiver coils in two dimensions and denote by $\boldsymbol{x} \in \Omega \subseteq \mathbb{R}^2$ the coordinates in the 2-D k-space. The relationship between the multi-coil images and the measurements acquired by the MRI scanner can be mathematically expressed as:

$$\boldsymbol{m}(\boldsymbol{x}) = \boldsymbol{E}\boldsymbol{u}(\boldsymbol{x}) + \boldsymbol{n}(\boldsymbol{x}). \quad (1)$$

Here, $\boldsymbol{u}(\boldsymbol{x}) = [u_1(\boldsymbol{x}) \dots u_M(\boldsymbol{x})] : \Omega \mapsto \mathbb{C}^M$ represents the vector-valued image consisting of the M coil images, $\boldsymbol{E}$ is the Fourier sampling operator, which is defined according to the k-space trajectory that is utilized, and $\boldsymbol{n}(\boldsymbol{x})$ is a complex-valued Gaussian term which accounts for all possible errors during MRI acquisition, such as scanner imprecisions and stochastic measurement noise. Each one of the coil images, $u_i(\boldsymbol{x})$, can be further written as:

$$u_i(\boldsymbol{x}) = S_i(\boldsymbol{x})\tilde{u}(\boldsymbol{x}), \forall i = 1 \dots M \quad (2)$$

where $S_i(\boldsymbol{x})$ corresponds to the sensitivity function of the i-th MRI coil and $\tilde{u}(\boldsymbol{x})$ is the underlying image.

Based on the forward model of Eq. (1) and assuming that the complex Gaussian noise in the different coils is uncorrelated[1], the reconstruction of the multichannel data, $\boldsymbol{u}$, can be cast as the minimization of a cost functional of the form:

$$J\left(\boldsymbol{u}\right) = \frac{1}{2}\left\|\boldsymbol{m} - \boldsymbol{E}\boldsymbol{u}\right\|_2^2 + \tau R\left(\boldsymbol{u}\right). \tag{3}$$

The first term in Eq. (3) quantifies the proximity of the estimated data to the measurements, while the second term promotes certain favorable properties in $\boldsymbol{u}$. The regularization parameter $\tau \geq 0$ is used to balance the contribution of the two terms.

3. NON-LOCAL REGULARIZATION

Recently there has been an increasing research interest in the development of non-local regularization functionals that can model certain image properties. The main reason is that non-local variational techniques seem to have great potentials in capturing information about complex image structures and promoting reconstructions that exhibit the non-local self-similarity property. This has been supported by results in several imaging applications (see for example [3, 4, 5]).

Among the best representatives of this class of regularization functionals is the non-local Total Variation (NLTV) introduced in [4]. The definition of NLTV is directly related to the notion of non-local differential operators. We note that while its original definition considers real functions/images, the extension of NLTV to also cover complex-valued functions is straightforward. Let $u\left(\boldsymbol{x}\right)$ be a complex-valued function $u : \Omega \mapsto \mathbb{C}$. Then, the non-local gradient of u evaluated at $\boldsymbol{x}$, $\nabla_w u\left(\boldsymbol{x}\right) : \Omega \mapsto \Omega \times \Omega$, is defined as the vector of all partial derivatives

$$\nabla_w u\left(\boldsymbol{x}, \boldsymbol{y}\right) = \left(u\left(\boldsymbol{y}\right) - u\left(\boldsymbol{x}\right)\right)\sqrt{w\left(\boldsymbol{x}, \boldsymbol{y}\right)}, \ \boldsymbol{x}, \boldsymbol{y} \in \Omega, \tag{4}$$

where $w\left(\boldsymbol{x}, \boldsymbol{y}\right) : \Omega \times \Omega \mapsto \mathbb{R}_+$ is a non-negative and symmetric weight function, i.e., $w\left(\boldsymbol{x}, \boldsymbol{y}\right) = w\left(\boldsymbol{y}, \boldsymbol{x}\right)$. In the context of non-local differential operators another very useful operator is the non-local divergence, $\mathrm{div}_w\vec{v} : \Omega \times \Omega \mapsto \Omega$, which corresponds to the negative adjoint of the non-local gradient and can be computed as

$$\left(\mathrm{div}_w\vec{v}\right)\left(\boldsymbol{x}\right) = \int_\Omega \left(v\left(\boldsymbol{x}, \boldsymbol{y}\right) - v\left(\boldsymbol{y}, \boldsymbol{x}\right)\right)\sqrt{w\left(\boldsymbol{x}, \boldsymbol{y}\right)}d\boldsymbol{y}. \tag{5}$$

Based on this non-local framework, Gilboa and Osher defined the NLTV functional in [4] as:

$$\mathrm{NLTV}\left(u\right) = \int_\Omega \left\|\nabla_w u\left(\boldsymbol{x}\right)\right\|_2 d\boldsymbol{x}. \tag{6}$$

The choice of the non-local weights $w\left(\boldsymbol{x}, \boldsymbol{y}\right)$ plays a central role in the definition of NLTV. The strategy for computing these weights is inspired by the non-local means filtering [6] which has been introduced for image denoising. In particular, the weight that links a pair of image points $\left(\boldsymbol{x}, \boldsymbol{y}\right)$ is computed by comparing the distance of two patches centered on the image points of interest. A widely used formula for the weight computation is given by

$$w\left(\boldsymbol{x}, \boldsymbol{y}\right) = e^{-\int_\Omega \frac{G(\boldsymbol{t})|u(\boldsymbol{x}+\boldsymbol{t}) - u(\boldsymbol{y}+\boldsymbol{t})|^2}{h^2}d\boldsymbol{t}}, \tag{7}$$

where G is a windowing function, such as a Gaussian kernel, and h is a filtering parameter.

---

[1]This assumption is not restrictive since in the case of correlated noise a whitening process of the measurements can take place as a preprocessing step.

3.1. Vectorial NLTV

The above definition of NLTV applies to single-channel images. In our case we wish to regularize the multi-coil image and therefore we need to adjust the definition of NLTV to suit our needs. To do so, we first note that the M coil images are highly correlated. This is clear by inspecting Eq. (2) and observing that each of the coil images corresponds to a component-wise product of the sensitivity map of the respective coil and the underlying image $\tilde{u}$. We also note that the sensitivity maps of the coils typically have a spatial overlap and they are varying smoothly. Based on the above, we propose to employ the following vectorial version of NLTV

$$\mathrm{VNLTV}\left(\boldsymbol{u}\right) = \int_\Omega \left(\sum_{m=1}^M \left\|\nabla_w u_m\left(\boldsymbol{x}\right)\right\|_2^2\right)^{\frac{1}{2}} d\boldsymbol{x}. \tag{8}$$

We note that the way our proposed penalty imposes a dependency among the data is twofold. First, it introduces a coupling between the different channels (coil images) and second it employs the same non-local weights in all channels. We compute these weights from a single-channel image that results as the root-sum-of-squares (RSoS) of the back-projected measurements. Our choice for using common non-local weights is motivated by the fact that all the coil images contain the same structural information which is determined from the unique underlying image $\tilde{u}$.

4. PARALLEL MRI RECONSTRUCTION

Since in practice we have to deal with discrete measurements, hereafter we will focus on the discrete version of the MRI reconstruction problem. In this case the multi-coil data $\boldsymbol{u}$ correspond to a complex vector of size $N \cdot M \times 1$, where N is the number of pixels of each coil image u_i, $\boldsymbol{E} \in \mathbb{C}^{KM \times NM}$ with $K < N$, is the MRI system matrix and $\boldsymbol{m}$ is a complex vector of size $K \cdot M \times 1$ consisting of the measurements.

Based on the discrete counterpart of the pMRI observation model in (1) and under the vectorial NLTV regularization (8), a penalized maximum likelihood (ML) estimate $\boldsymbol{u}^\star$ of the multi-coil data is obtained as the minimizer

$$\boldsymbol{u}^\star = \arg\min_{\boldsymbol{m} \in \mathbb{C}^{N \cdot M}} \frac{1}{2}\left\|\boldsymbol{m} - \boldsymbol{E}\boldsymbol{u}\right\|_2^2 + \tau\left\|\nabla_w\boldsymbol{u}\right\|_{1,F}, \tag{9}$$

where $\left(\nabla_w\boldsymbol{u}\right)_n = \left[\left(\nabla_w u_1\right)_n \ldots \left(\nabla_w u_M\right)_n\right] \in \mathbb{C}^{L \times M}$ is a matrix formed by stacking in its ith column the non-local gradient of u_i evaluated at the nth pixel, which is a vector of size L, and $\left\|\cdot\right\|_{1,F}$ is a mixed vector-matrix norm defined as

$$\left\|\nabla_w\boldsymbol{u}\right\|_{1,F} = \sum_{n=1}^N \left\|\left(\nabla_w\boldsymbol{u}\right)_n\right\|_F, \tag{10}$$

with $\left\|\cdot\right\|_F$ being the Frobenius norm.

The main difficulties in obtaining the minimizer of Eq. (9) are the non-smoothness of the VNLTV regularizer, which does not allow us to employ a gradient descent scheme, and the coupling that exists between the two terms of the objective function. To deal with this problem, we introduce the auxiliary variable $\boldsymbol{z} = \nabla_w\boldsymbol{u} \in \mathcal{X} = \mathbb{C}^{N \times L \times M}$ and express (9) in the equivalent constrained form

$$\min_{\substack{\boldsymbol{m} \in \mathbb{C}^{N \cdot M} \\ \boldsymbol{z} = \nabla_w\boldsymbol{u}}} \underbrace{\frac{1}{2}\left\|\boldsymbol{m} - \boldsymbol{E}\boldsymbol{u}\right\|_2^2}_{f(\mathbf{u})} + \underbrace{\tau\left\|\boldsymbol{z}\right\|_{1,F}}_{g(\boldsymbol{z})}. \tag{11}$$

Algorithm 1 : Parallel MRI reconstruction.

Input: m, E, $\tau > 0$, $\alpha > 0$

Initialization: $u^0 = F^H m$, $s^0 = 0$, $t = 0$.

while *stopping criterion is not satisfied* **do**

$\quad z_n^{t+1} \leftarrow S_{\tau/\alpha}\left(\left(\nabla_w u^t\right)_n + s_n^t\right);$

$\quad A \leftarrow \left(E^H E - \alpha \mathrm{div}_w \nabla_w\right);$

$\quad u^t \leftarrow A^{-1}\left(E^H m - \alpha \mathrm{div}_w\left(z^{t+1} - s^t\right)\right);$

$\quad s^t \leftarrow s^t + \nabla_w u^{t+1} - z^{t+1};$

$\quad t \leftarrow t + 1;$

end

$\tilde{u}^\star = \left(\sum_{m=1}^{M} u_m{}^H u_m\right)^{1/2};$

return $\tilde{u}^\star;$

Table 1. nRMSE comparisons on pMRI reconstruction for various noise levels and reduction factors (RF) using two sampling masks.

			RF=5			RF=6			RF=7		
		SNR	5dB	10dB	15dB	5dB	10dB	15dB	5dB	10dB	15dB
Brain image	RVD	CLEAR	3.93E-2	2.71E-2	2.16E-2	3.71E-2	2.67E-2	2.21E-2	3.82E-2	2.86E-2	2.40E-2
		SPIRiT	3.22E-2	2.08E-2	1.66E-2	3.08E-2	2.12E-2	1.77E-2	3.06E-2	2.26E-2	1.94E-2
		VNLTV	2.18E-2	1.81E-2	1.61E-2	2.23E-2	1.87E-2	1.72E-2	2.36E-2	2.00E-2	1.88E-2
	PVD	CLEAR	4.17E-2	2.68E-2	1.99E-2	4.11E-2	2.80E-2	2.16E-2	4.12E-2	2.92E-2	2.31E-2
		SPIRiT	3.46E-2	2.03E-2	1.48E-2	3.28E-2	2.08E-2	1.60E-2	3.23E-2	2.17E-2	1.74E-2
		VNLTV	2.18E-2	1.77E-2	1.52E-2	2.33E-2	1.94E-2	1.74E-2	2.47E-2	2.11E-2	1.95E-2
Knee image	RVD	CLEAR	4.99E-2	3.42E-2	2.62E-2	4.85E-2	3.49E-2	2.83E-2	5.04E-2	3.82E-2	3.19E-2
		SPIRiT	4.79E-2	3.14E-2	2.35E-2	4.68E-2	3.25E-2	2.60E-2	4.75E-2	3.46E-2	2.84E-2
		VNLTV	3.02E-2	2.48E-2	2.16E-2	3.08E-2	2.61E-2	2.37E-2	3.36E-2	2.89E-2	2.67E-2
	PVD	CLEAR	5.05E-2	3.11E-2	2.10E-2	4.94E-2	3.24E-2	2.33E-2	4.99E-2	3.46E-2	2.62E-2
		SPIRiT	4.89E-2	2.85E-2	1.85E-2	4.68E-2	2.89E-2	2.01E-2	4.64E-2	3.05E-2	2.25E-2
		VNLTV	2.84E-2	2.23E-2	1.83E-2	3.07E-2	2.47E-2	2.11E-2	3.31E-2	2.73E-2	2.44E-2

Now, since we have transformed our original problem to a constrained minimization, we can solve it by forming the augmented Lagrangian and employing the ADMM/Split Bregman algorithm [7, 8]. We recall that ADMM solves problems of the generic form,

$$\min_{Au+Bz=c} f(u) + g(z) \qquad (12)$$

which covers our problem as a special case by setting $A = \nabla_w$, $B = -I$, and $c = 0$.

Ignoring irrelevant constants to the optimization task, the augmented Lagrangian associated to Problem (11) can be written as:

$$\mathcal{L}_\alpha(u, z, s) = f(u) + g(z) + \frac{\alpha}{2}\|\nabla_w u - z + s\|_\mathcal{X}^2 \qquad (13)$$

where $s = \eta/\alpha$ are the scaled Lagrange multipliers and $\alpha > 0$ is a penalty parameter. Now, it is easy to show that the ADMM iterations that solve (11) are given by

$$z^{t+1} = \arg\min_z \frac{1}{2}\left\|z - \left(\nabla_w u^t + s^t\right)\right\|_\mathcal{X}^2 + \frac{\tau}{\alpha}\|z\|_{1,F} \qquad (14a)$$

$$u^{t+1} = \arg\min_u \|m - Eu\|_2^2 + \alpha\left\|\nabla_w u - \left(z^{t+1} - s^t\right)\right\|_\mathcal{X}^2 \qquad (14b)$$

$$s^{t+1} = s^t + \nabla_w u^{t+1} - z^{t+1}. \qquad (14c)$$

To solve subproblem (14a) we first note that by using (10) we can express its argument as:

$$\sum_{n=1}^{N} \frac{1}{2}\left\|z_n - \left(\left(\nabla_w u^t\right)_n + s_n^t\right)\right\|_F^2 + \frac{\tau}{\alpha}\|z_n\|_F$$

and, thus, we can compute each z_n^{t+1} independently as

$$z_n^{t+1} = S_{\tau/\alpha}\left(\left(\nabla_w u^t\right)_n + s_n^t\right). \qquad (15)$$

In Eq. (15) S_γ corresponds to a shrinkage function that accepts a complex matrix X as an argument and is defined as

$$S_\gamma(X) = \max\left(\|X\|_F - \gamma, 0\right)\frac{X}{\|X\|_F}. \qquad (16)$$

The subproblem (14b) is a quadratic one and thus the minimizer can be obtained by solving the following system of linear equations:

$$\left(E^H E - \alpha \mathrm{div}_w \nabla_w\right) u^{t+1} = \left(E^H m - \alpha \mathrm{div}_w\left(z^{t+1} - s^t\right)\right). \qquad (17)$$

Since the inversion of the matrix in the l.h.s of (17) is prohibitive due to its large size, we employ instead the conjugate gradient (CG) method [9]. We have experimentally observed that if we choose the starting point of CG to be the solution of the quadratic sub-problem of the previous ADMM iteration ("warm-start" strategy), then as few as two CG iterations suffice for the convergence of the overall algorithm.

A summary of our overall reconstruction approach is provided in Algorithm 1.

5. EXPERIMENTS

In this section we report reconstruction results on two 8-channel k-space datasets of a brain and knee, which are shown in Fig. 1(a) and Fig. 2(a), respectively. These data were retrospectively under-sampled using two different sampling masks, namely a Poisson-Disk (PD) variable density and a random variable density mask at reduction factors (RF) of 5 - 7. All k-space data retained a 24×24 fully sampled central region. Besides the under-sampling, we also considered three different levels of i.i.d complex Gaussian noise degrading the fully sampled k-space measurements. These noise levels correspond to signal-to-noise-ratios (SNRs) of 5, 10, and 15 dBs, respectively.

To assess the performance of our pMRI reconstruction approach we compared it with two alternative pMRI methods, namely CLEAR [2] and L_1-SPIRiT [10]. CLEAR is an image-domain pMRI method that imposes a locally low-rank constraint on the multi-coil images, while L_1-SPIRiT is a k-space based method that enforces both a calibration consistency constraint and wavelet sparsity. The latter method similarly to VNLTV and CLEAR does not require knowledge of the coil sensitivities, but still uses an auto-calibration region. This is also the reason that in our comparisons we consider sampling patterns that retain a fully sampled central region.

Regarding the implementation details of the methods under study, the patch-size for the computation of the non-local weights of VNLTV was set to 7×7 and the size of the search window (constant windowing function) to 11×11. For the minimization of VNLTV we run 50 iterations of the algorithm described in Algorithm 1. The patch size for CLEAR was set to 8×8 and the
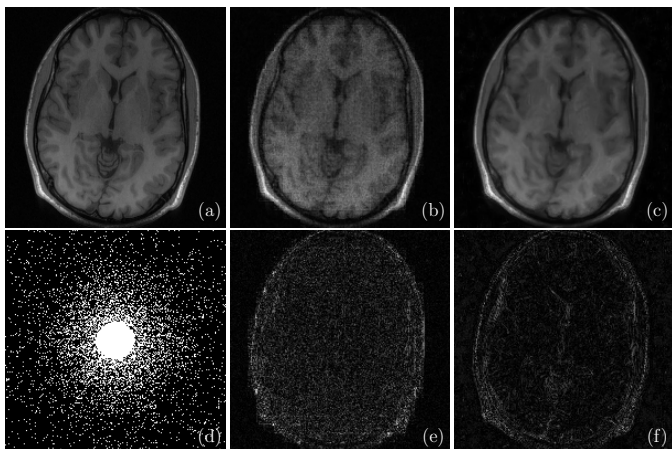
Fig. 1. Reconstruction results of a brain image for a reduction factor 7 and SNR=10 dB. (a) Fully-sampled and noise-free result, (b) CLEAR (nRMSE=2.86E-2), (c) VNLTV (nRMSE=2.00E-2), (d) random variable density sampling pattern, (e) error map for CLEAR, (f) error map for VNLTV.

Fig. 2. Reconstruction results of a knee image for a reduction factor 6 and SNR=10 dB. (a) Fully-sampled and noise-free result, (b) SPIRiT (nRMSE=2.87E-2), (c) VNLTV (nRMSE=2.47E-2), (d) Poisson-disk variable density sampling pattern, (e) error map for SPIRiT, (f) error map for VNLTV.

thresholding parameters were adaptively adjusted (per iteration) to be proportional to the median magnitude of the transform domain coefficients. The number of iterations for the minimization of the corresponding objective function was set to 50. Finally, the kernel size for L1-SPIRiT was set to 5×5 and the ℓ_1-norm penalty was imposed on Daubechies wavelet coefficients. The L1-SPIRiT reconstruction was performed using a Projection-Onto-Convex-Set (POCS) algorithm with a maximum of 50 iterations.

In Table 1 we report the reconstruction results of all the three methods under comparison. The quality of the reconstructions is measured in terms of normalized root mean squared error (nRMSE). From these results we observe that especially for high and medium levels of noise, corresponding to SNRs of 5 and 10 dBs, respectively, our method consistently outperforms the other two methods regardless the reduction factor and the sampling mask, while for lower levels of noise our method is still very competitive. Apart from the quantitative comparisons, the effectiveness of our proposed approach can also be visually appreciated by inspecting the representative examples shown in Figs. 1 and 2. These results confirm that our method is robust and leads to satisfactory reconstructions even for high reduction factors and noise conditions.

6. CONCLUSIONS

We proposed a variational framework for a calibration-free pMRI reconstruction that exploits the non-local self-similarity property of natural images and the correlation between the different MRI coil images. This is accomplished by employing a vectorial counterpart of the non-local total variation regularizer. Our method compares favorably with alternative pMRI techniques and shows significant advantages especially when the measurements are contaminated by high levels of noise.

7. REFERENCES

[1] P. Shin, P. Larson, M. Ohliger, M. Elad, J. Pauly, D. Vigneron, and M. Lustig, "Calibrationless parallel imaging reconstruction based on structured low-rank matrix completion," *Magnetic Resonance in Medicine*, 2013.
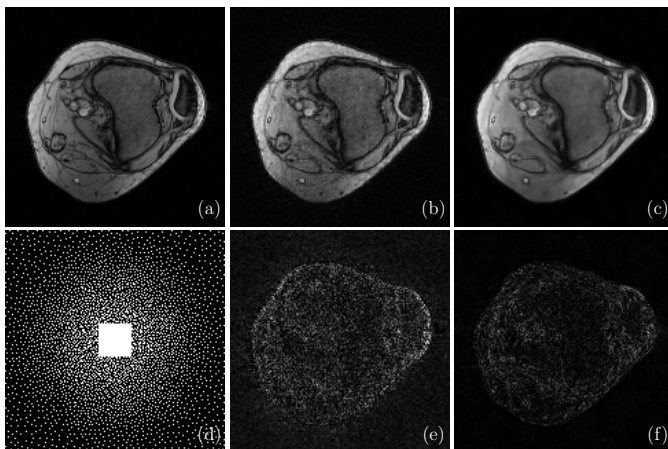
[2] J. Trzasko and A. Manduca, "Calibrationless parallel mri using clear," in *IEEE Asilomar Conference on Signals, Systems and Computers*, 2011, pp. 75–79.

[3] A. Elmoataz, O. Lezoray, and S. Bougleux, "Nonlocal discrete regularization on weighted graphs: a framework for image and manifold processing," *IEEE Trans. Image Proces.*, vol. 17, pp. 1047–1060, 2008.

[4] G. Gilboa and S. Osher, "Nonlocal operators with applications to image processing," *Multiscale Model. Simul.*, vol. 7, pp. 1005–1028, 2008.

[5] G. Peyré, S. Bougleux, and L. Cohen, "Non-local regularization of inverse problems," *Inverse Problems and Imaging*, vol. 5, pp. 511–530, 2011.

[6] A. Buades, B. Coll, and J.-M. Morel, "Image denoising methods. A new nonlocal principle," *SIAM review*, vol. 52, pp. 113–147, 2010.

[7] E. Esser, "Applications of Lagrangian-based alternating direction methods and connections to split Bregman," *CAM report*, vol. 9, 2009.

[8] T. Goldstein and S. Osher, "The split Bregman method for L_1-regularized problems," *SIAM J. Imaging Sci.*, vol. 2, pp. 323–343, 2009.

[9] J. R. Shewchuk, "An introduction to the conjugate gradient method without the agonizing pain," 1994.

[10] M. Lustig and J. Pauly, "Spirit: Iterative self-consistent parallel imaging reconstruction from arbitrary k-space," *Magnetic Resonance in Medicine*, vol. 64, no. 2, pp. 457–471, 2010.